NOTICE

CERTAIN DATA CONTAINED IN THIS DOCUMENT MAY BE DIFFICULT TO READ IN MICROFICHE PRODUCTS.

COMPARISON OF THE EFFECTS OF LONG-TERM THERMAL AGING AND HFIR IRRADIATION ON THE MICROSTRUCTURAL EVOLUTION OF 9Cr-1MoVNb STEEL

P.J. Maziasz and R.L. Klueh

Metals and Ceramics Division
Oak Ridge National Laboratory
P.O. Box 2008, Oak Ridge, Tn 37831-6376

CONF-900623--22

DE91 004516

ABSTRACT

Both thermal aging at 482-704°C for up to 25,000h and HFIR irradiation at 300-600°C for up to 39 dpa produce substantial changes in the as-tempered microstructure of 9Cr-1MoVNb martensitic/ferritic steel. However, the changes in the dislocation/subgrain boundary and the precipitate structures caused by thermal aging or neutron irradiation are quite different in nature. During thermal aging, the as-tempered lath/subgrain boundary and carbide precipitate structures remain stable below 650°C, but coarsen and recover somewhat at 650-704°C. The formation of abundant intergranular Laves phase, intra-lath dislocation networks, and fine dispersions of VC needles are thermal aging effects that are superimposed upon the as-tempered microstructure at 482-593°C. HFIR irradiation produces dense dispersions of very small "black-dot" dislocations loops at 300°C and produces helium bubbles and voids at 400°C. At 300-500°C, there is considerable recovery of the as-tempered lath/subgrain boundary structure and microstructural/microcompositional instability of the as-tempered carbide precipitates during irradiation. By contrast, the as-tempered microstructure remains essentially unchanged during irradiation at 600°C. Comparison of thermally aged with irradiated material suggests that the instabilities of the as-tempered lath/subgrain boundary and precipitate structures at lower irradiation temperatures are radiation-induced effects, whereas

DISCLAIMER

the absence of both Laves phase and fine VC needles during irradiation is a radiation-retarded thermal effect.

INTRODUCTION

Since the early 1970's, there has been increased world wide interest in the use of 9-12 Cr martensitic/ferritic steel as alternatives to austenitic stainless steels for elevated temperature applications up to about 600°C in both nuclear and fossil energy systems [1-4]. The 9Cr-1MoVNb steel was developed jointly by the Oak Ridge National Laboratory (Oak Ridge, TN) and Combustion Engineering (Chattanooga, TN) in response to the mandate in 1974 by the U.S. Liquid Metal Fast Breeder Reactor (LMFBR) Materials Program for a better steam generator material [1, 5, 6]. Also designated T-91, this steel offers better tensile and creep strength at 600°C relative to standard 9Cr-1Mo (F9) or other modified 9Cr steels (ie. 9Cr-2MoVNb or EM-12) with better impact properities at lower temperatures [6]. Because the martensitic/ferritic class of steels also demonstrate outstanding resistance to radiation-induced void swelling [7-10], these steels have also been considered for in-core LMFBR applications. Void swelling resistance plus good thermal conductivity and low thermal expansion have made 9Cr-1MoVNb an attractive candidate first-wall material for Magnetic Fusion Reactor (MFR) applications as well [11, 12].

Many of the mechanical properties limitations that occur during long-term thermal aging or neutron irradiation of 9Cr martenisitic/ferritic steels can be related to changes in the as-tempered microstructure caused by such exposure. Long-term aging of 9Cr-1Mo steel produces embrittlement by increasing the ductile-to-brittle transition temperature (DBTT), which can be related to Laves phase precipitation along grain boundaries [13-15]. Radiation-induced increases

of DBTT in 9-12Cr steels appear caused by matrix hardening related to a variety of fine, radiation-produced microstructural defects [16-20].

The purpose of this paper is to characterize the microstructural evolution of 9Cr-1MoVNb steel after irradiation in HFIR at 300-600°C to 37-39 dpa (about 10,000h) and after long-term thermal aging at 482-704°C for 10,000 and 25,000h. Particular emphasis is given to characterization of the precipitate component of the microstructure using analytical electron microscopy (AEM). The comparison of the long-term aging data with reactor-irradiation data allows radiation-induced microstructural changes to be separated from those that are radiation-enhanced, -modified or -retarded thermal effects. Correct phenomenological assessment combined with microstructure-properties correlations in future work can provide insight to guide further optimization of 9Cr-1MoVNb steels for either nuclear or non-nuclear applications.

EXPERIMENTAL

The compositions of two heats (30176 and 30394) of 9Cr-1MoVNb steel produced by Carpenter Technology (CarTech) and one heat (XA 3590) produced by Combustion Engineering (CE, Cattanooga, TN), which were investigated in this work, are given in Table 1. The major difference is that heats 30176 and XA 3590 both contain less Si than heat 30394, but all fall within the T-91 specification [6]. All of the steels were finished in a normalized (0.5 h at 1040°C, He quenched to room temperature) and tempered (1h at 760°C) condition. Tensile, creep and Charpy-impact specimens were fabricated from plate-stock of heats 30176 and 30394 and aged stress-free at 482, 538, 593, 650 and 706°C for 10,000 and 25,000h. Material of heat XA 3590 was first processed into 0.25-mm thick sheet stock from which standard 3-mm diameter

transmission electron microscopy (TEM) disks were punched. These disks were then also normalized and tempered prior to irradiation in the HFIR-CTR-30 experiment. Disks were irradiated at temperatures of 300, 400, 500 and 600°C to fluences of fast and thermal neutrons that produced 36.5 to 38.5 dpa and 30-32 at. ppm He in about 10,000h.

TEM disks were punched from slices cut from thermally aged tensile (shoulder) or Charpy-impact specimens. Precipitates were electrolytically extracted onto carbon films from the TEM disks prior to electropolishing, and suspended on either copper, beryllium or carbon-coated nylon grids for analysis using x-ray energy dispersive spectroscopy (XEDS). The remainder of the slice was used for bulk electrolytic extraction of precipitates to quantitatively measure the weight fraction of residue. Only extraction replica and thin-foil specimens could be made from the highly radioactive HFIR-irradiated TEM disks.

Thin-foil specimens were examined using a JEM 100C TEM equipped with an AMG objective lens pole piece to minimize ferromagnetic displacements and stigmatism of the electron beam. Phase identification and quantitative microcompositional analysis of both individual particles and large areas with thousands of particles (broad-beam analysis) on the replica specimens were performed using a Philips EM400T/FEG (100 KV, field-emission gun, with <10 nm probe size) AEM with an EDAX 9100 analysis unit and a JEM 2000FX (200 KV, LaB_6 gun) AEM with a TN-5500 Series II analysis unit. Only the normallized composition of metallic elements heavier than Al were analyzed using XEDS. More details concerning analysis techniques can be found elsewhere [21-24].

RESULTS

As-Tempered Microstructure of 9Cr-1MoVNb

The as-tempered microstructure of both heats of 9Cr-1MoVNb martensitic/ferritic steel consisted of small intragranular lath-shaped ferrite subgrains within larger grains from prior austenite (Fig 1a). Tempering produced about 1.4-1.8 wt.% precipitation [25] (Table 2), distributed as mainly coarse $M_{23}C_6$ and some finer MC particles along grain and lath/subgrain boundaries (Fig 1b). XEDS analysis of individual precipitate particles extracted onto carbon replica films showed Cr-rich $M_{23}C_6$ and V- and Nb-rich MC phases (Fig. 1b). Quantitative broad beam XEDS analysis indicated that 85-90 vol.% of the extracted precipitates were $M_{23}C_6$ and 10-15% were MC, with most of the MC particles being VC. The as-tempered lath/subgrains contained dislocation networks, with densities that varied from 1-7 $\times$ 10^{13} m^{-2} in larger subgrains to less in smaller ones. The lath/subgrain boundaries were also planar honeycomb arrays of dislocations with a much higher density.

Microstructural Evolution of 9Cr-1MoVNb During Thermal Aging

Microstructural changes were observed in the 9Cr-1MoVNb steel at all aging temperatures in the range of 482-704°C after 25,000h. The data can easily be separated into two temperature regimes of quite different aging effects. At the lower temperatures of 482-593°C, there was little change in the as-tempered lath/boundary and carbide precipitate structures, while at 650 and 704°C, there was detectable recovery and coarsening of the lath/subgrain boundary structure, and coarsening of the as-tempered carbide precipitates. A considerable amount of new precipitation and an increase in the concentration of dislocation networks were observed within subgrains in the lower temp-

erature regime, while no new precipitate phases were observed at 650 and 704°C in the lower Si heat of steel (Table 2).

Dislocation density within many subgrains increased during aging at 538°C for 25,000h relative to the as-tempered material (Fig. 2a and 2b). By contrast, aging for 25,000h at 650°C produced almost no change in microstructure relative to as-tempered material (Fig. 2c). Aging for 25,000h at 704°C caused recovery and coarsening of the as-tempered lath subgrain structure into larger, equiaxed subgrains (cp. Figs. 1a and 3). Quantitative data on the weight percent of extracted precipitation from Table 2 are plotted in Fig. 4a. The amount of precipitation showed a significant increase at the lower aging temperatures.

Both thin-foil TEM and quantitative AEM analysis on extraction replicas revealed abundant Laves phase formation (Fe_2Mo type) during aging. Quantitative data from XEDS broad-beam and individual particle analyses on extraction replicas are given in Tables 3 and 4, respectively. Laves phase is highly enriched in molybdenum, and contains much more molybdenum than the carbide phases. Therefore, Laves phase is best detected by monitoring the molybdenum content of the broad-beam XEDS spectra. Correlation of broad-beam molybdenum content (also plotted as a function of aging temperature in Fig. 4b) with the weight fraction of precipitate demonstrates that the increase in precipitation during aging was due mainly to the formation of Laves phase.

Below 600°C, significantly more Laves phase was found in the heat of 9Cr-1MoVNb with more silicon (heat 30394) than in the lower silicon heat (heat 30176) (Fig. 4a). The Laves phase composition did not show significant temperature dependence in either heat of steel. However, the Laves phase composition is lower in molybdenum and higher in silicon in the high silicon

heat of steel (Table 4). No Laves phase was observed in the lower silicon heat of steel at 650°C after 25,000h. By contrast, while no Laves phase was observed in the higher silicon steel after 10,000h at 650°C, a large amount of Laves precipitated after 25,000h.

Laves phase was microstructurally distributed as thin films along grain and subgrain boundaries at 482 and 538°C (Figs. 5 and 6). Laves phase formed as coarser particles at 593 and/or 650°C. In the higher silicon heat of steel, Laves phase often formed as massive, globular particles that engulfed coarse boundary carbide particles at 482 and 538°C (Fig. 6b), and as boundary films.

Fine VC needles were also produced by aging at 482-593°C for 25,000h in both heats of steel, but not at 650°C and above. Fine needles were also detected in the low-silicon heat of steel after 10,000h at 538°C. The fine VC precipitates were distributed uniformly within larger lath/subgrains, but were heterogeneously distributed on a coarser scale because groups or packets of cells would have them while others would not. They were detectable only with higher-magnification TEM, both in thin-foil and on extraction replica specimens, as shown in Fig. 7, because they made virtually no contribution to the weight fraction of extracted precipitate or the XEDS broad-beam spectra. Compositionally, they were very similar to the larger VC precipitates, although often they had slightly more chromium and less vanadium (Table 5).

The major changes produced by aging at 650°C and above were structure recovery and precipitate coarsening, particularly at 704°C after 25,000h (Fig. 3). Although the total weight fraction of precipitate remains about equal to that produced during tempering, both TEM and AEM analysis of extraction replicas indicated coarsening of the carbide precipitates, particularly the MC particles [26]. Broad-beam analysis at 704°C indicates an increase in the

relative volume fraction of MC to $M_{23}C_6$ phases compared to the as-tempered material (more V and Nb, Table 3). While neither carbide phase showed any significant compositional change when they were stable at lower aging temperatures, both showed detectable compositional changes when they become unstable at 650-704°C. The $M_{23}C_6$ phase (average as-tempered composition-62%Cr-29%Fe-5.5%Mo-1%V, with detectable Si, Nb and Mn as well) contained slightly more chromium and less iron at 650 and 704°C. The VC particles become richer in niobium at the expense of chromium and vanadium at 704°C relative to the as-tempered condition (Table 5), and the fraction of mixed V- and Nb-rich MC particles also appeared to increase.

Microstructural Evolution of 9Cr-1MoVNb During HFIR Irradiation

Microstructural changes due to irradiation of the low-silicon heat of 9Cr-1MoVNb in HFIR to 37-39 dpa (about 10,000h) were observed primarily at 300-500°C; irradiation at 600°C produced almost no change relative to the as-tempered microstructure. Radiation-induced dislocation loop and void formation were confined to very narrow ranges of temperature. Tiny "black-dot" dislocation loop damage was observed only at 300°C (Fig. 8), while helium bubbles and voids were only observed to form at 400°C (Fig. 9). By contrast, changes in matrix dislocation concentration, lath/subgrain boundary structure, and carbide distribution and composition occurred as continuous functions of irradiation temperature from 300 to 500°C.

The matrix dislocation density of the 9Cr-1MoVNb steel irradiated in HFIR followed a normal temperature dependence, with the highest dislocation concentration (a mixture of loops plus network) at 300°C (Fig. 8d), less at 400 and 500°C (network only)(Figs. 9a and 10), and the lowest concentration at

600°C (Fig. 11). Quantitative measurements of dislocation concentration showed the network after irradiation at 400°C falling consistently to the higher side of the wide range observed in as-tempered material (6×10^{13} and $<1\text{-}7 \times 10^{13}$ m^{-3}, respectively [24]). The concentration of dislocation networks after HFIR irradiation at 500 and 600°C was very similar to that found in the as-tempered condition

While the radiation-produced dislocation density followed a normal temperature dependence, recovery and coarsening of the as-tempered lath/subgrain boundary structure was observed to follow an inverse temperature dependence during HFIR irradiation at 300-500°C. Recovery of the cellular subgrain structure was greatest at 300°C (Fig. 8) and least at 500°C, and at 600°C there was no discernable difference between HFIR-irradiated and as-tempered material (Figs. 8b and 11). Evidence for recovery of the subgrain structure is best seen from comparison of lower and higher magnification TEM of an as-tempered specimen with one irradiated in HFIR at 300°C in Fig. 8. At higher magnification, the small cell boundaries, which often consist of dense honeycombe networks, were a dominant microstructural feature in as-tempered material, but were almost completely absent after HFIR irradiation at 300°C (cp. Fig. 8b and 8d). Many large regions of matrix were also free of subgrain structure after irradiation at 400°C (Fig. 9a) [24]. After irradiation at 500°C most of the initial subgrain boundary structure remained (Fig. 10), but subgrain size was slightly coarser than found in either as-tempered material or material irradiated at 600°C. One subtle hint that irradiation at 500°C had altered the structure is the fact that many carbide precipitate particles were not associated with boundaries, as was the case in as-tempered material. At lower magnification, it can be seen that coarser packet bound-

aries established during tempering and prior austenite grain boundaries (both usually heavily decorated with carbide precipitates) were still visible after irradiation at 300°C (Fig. 8a and 8c).

HFIR irradiation produced no new precipitate phases in the 9Cr-1MoVNb steel (Table 6). There were, however, changes in the as-tempered carbide structure that were parallel to the recovery and coarsening of the lath/subgrain boundary structure, particularly in terms of temperature dependence. Microstructurally, there appeared to be dissolution of many of the smaller $M_{23}C_6$ particles during irradiation at 300 and 400°C (Figs. 8d and 9a), which were associated with the lath/subgrain boundary structure in the as-tempered condition. Most of the coarser $M_{23}C_6$ particles decorating packet boundaries or prior austenite grain boundaries appeared unaffected by the irradiation, even at 300°C (Fig. 8c). Partial dissolution of $M_{23}C_6$ carbides exhibited the same inverse temperature dependence during irradiation as found for recovery and coarsening of the lath/subgrain boundary structure. Dissolution of small $M_{23}C_6$ particles was most noticeable at 300 and 400°C, but did not appear to be occuring at 500 and 600°C. Despite these changes in precipitate microstructure, XEDS studies of extraction replicas indicated no change of the $M_{23}C_6$ phase composition during irradiation over the temperature range of 300-600°C.

While the fine MC component of the precipitate structure was too difficult to observe consistently by TEM of the complex microstructure of the irradiated thin-foil specimens, significant microstructural and microcompositional changes caused by irradiation were observed by AEM analysis of these particles on extraction replica specimens. Previously, quantitative data showed that MC particle sizes ranged from 17 to 60 nm in the as-tempered material,

with more particles at the smaller end of the size range [24]. By comparison, the MC particle sizes ranged from 30 to 120 nm after HFIR irradiation at 400°C, with more particles at the larger side of the size range. The MC coarsening also had an inverse temperature dependence, because maximum effects of irradiation were observed at 300 and 400°C, while there was no detectable effect of irradiation at 600°C.

Irradiation dramatically changed the V and Cr concentrations of the MC phase particles in the 9Cr-1MoVNb steel, and this effect also had a strong, inverse temperature dependence. The pronounced increase in Cr at the expense of V that occurs in MC particles during HFIR irradiation at 400°C is shown clearly in Fig. 12. Irradiation appears to strongly affect only the V and Cr concentrations. This effect of irradiation on MC composition is similar for both V-rich or mixed V- and Nb-rich particles (Fig. 12). Both Table 7 and Fig. 13 show that the effect of irradiation on Cr and V content of MC particles was very stong at 300-500°C, but then becomes weaker at 600°C. The radiation-induced Cr-enrichment was maximum at 400°C and more temperature sensitive than V-depletion, which was greatest at 400-500°C. Clearly the MC composition during irradiation at 600°C moved much closer to the MC composition observed during thermal aging, although an effect of irradiation was still noticeable.

The XEDS broad beam compositions of extracted precipitates showed little difference after irradiation, except for irradiation at 300°C (Table 6). Given the MC phase composition produced during irradiation, analysis of the broad-beam data for relative phase fractions suggested a slight increase in the amount of MC relative to $M_{23}C_6$ at 300°C (17 and 83%, repectively). The amounts of MC relative to $M_{23}C_6$ in specimens irradiated at 400-600°C were

similar to that found in the as-tempered steel (10-12 and 88-90%, respectively). Bulk extraction measurements could not be performed on radioactive material, so quantitative changes in the total amount of precipitation could not be observed.

DISCUSSION

The data on 9Cr-1MoVNb steel indicate that the microstructural and microcompositional changes produced by HFIR irradiation and by thermal aging are quite different. However, it should also be obvious that the mechanisms driving such changes are also different in each exposure environment. The microstructural differences between thermally aged and HFIR irradiated 9Cr-1MoVNb steel can be summarized as follows: a.) the as-tempered subgrain boundary and precipitate structures are *stable* during aging at 600°C and below, but *unstable* during HFIR irradiation at 300-500°C; b.) Laves phase forms abundantly during aging below 600°C, but not at all during HFIR irradiation; c.) additional fine VC needles form during aging at 593°C and below, but not during HFIR irradiation; d.) the MC phase undergoes radical compositional changes during irradiation at 300-500°C that are not observed during aging at any temperature; e.) more dislocations are produced within the lath/subgrains during long-term thermal aging at 483-593°C than are produced during HFIR irradiation at 400-600°C. The radiation-induced loops at 300°C and cavities at 400°C are, of course, also important differences between aged and neutron-irradiated material. However, these microstructural features are the expected by-products of interstitial point-defects or helium atoms (from transmutation reactions) produced by neutron irradiation, and will not be discussed further here. Helium effects on bubble and void formation in 9 and

12 Cr steels irradiated in HFIR and FFTF have been extensively discussed elsewhere [24].

The instability of the as-tempered carbide precipitate and subgrain boundary structures and the compositional changes of the MC phase during HFIR irradiation at 300-500°C appear to be coupled microstructural phenomena. The inverse temperature dependence suggests that these are radiation-induced effects rather than radiation-enhanced thermal effects. Both the as-tempered MC particle distribution and subgrain boundary structure coarsen during long-term aging, but only at the highest temperatures. Both the degree of coarsening during lower-temperature irradiation and the associated dissolution of $M_{23}C_6$ particles and compositional changes of MC phase during coarsening (more Cr instead of less) also consistently point to phenomena that are radiation-induced and essentially non-thermal in nature. Moreover, there is a consistent correlation between changes of precipitate and subgrain boundary structures during aging and during irradiation. This would imply that the precipitates pin the boundaries so that subgrain boundaries cannot migrate unless the precipitates first become unstable. In fact, 12Cr-1MoVW steel similarly irradiated in HFIR at 300-500°C shows stability of both the as-tempered subgrain and carbide structures [24, 27], an opposite effect of irradiation relative to the 9Cr-1MoVNb steel, but consistent with precipitates preventing boundary migration. Thus, initial instability of the as-tempered carbides ($M_{23}C_6$ in particular) in the 9Cr-1MoVNb steel appears to be a root cause for the other microstructural changes observed during irradiation at 300-500°C.

In contrast to the radiation-induced aspects of microstructural evolution directly observed in 9Cr-1MoVNb steel irradiated in HFIR at 300-500°C, the

noticeable absence of both fine VC and coarser Laves phase precipitation suggests that irradiation has retarded these thermal phenomena. However, the failure of these dominant thermal precipitates to occur during irradiation can also be related indirectly to the instability of as-tempered carbides during irradiation. The last observation that seems intuitively strange is the increase in matrix dislocation concentration in aged compared to irradiated material. However, even this result can be explained in part by loop nucleation that is very strongly dependent on temperature combined with thermal dislocation network recovery processes occuring at an enhanced rate during irradiation of the 9Cr-1MoVNb steel.

Microstructural evolution during irradiation is generally caused by several mechanisms acting in concert, including: a.) cascade damage and point-defect production, b.) annihilation, accumulation and/or migration of radiation-produced point defects, and c.) radiation-induced segregation (RIS) and radiation-enhanced diffusion, both of which are caused by the fluxes of radiation-produced point defects. Microstructural changes during thermal aging are usually driven by solute supersaturation and diffusion, and dislocation/-boundary structure recovery processes.

It seems reasonable that the as-tempered microstructure established at high temperatures should be resistant to recovery during long-term aging at lower temperatures. The formation of fine VC carbides during aging below 600°C apparently indicates that the decrease in the carbon solubility with decreasing aging temperature produces a new carbon supersaturation (relative to that relieved by tempering), which then triggers additional carbide precipitation. The fine distribution of VC needles is consistent with nucleation on the increased number of dislocations available at the lower aging temperatures.

The formation of Laves phase as films along grain boundaries or as crusts around carbide particles would indicate that localized carbon depletion triggers the formation of this carbon-free intermetallic phase [28, 29]. The increase in the amount of Laves phase in the higher silicon heat of 9Cr-1MoVNb steel is consistent with silicon acting as a catalyst for the formation of that phase [28, 29].

Processes involving radiation-produced point defect are almost certainly the cause of the radiation-induced microstructural changes observed in 9Cr-1MoVNb steel, although several different mechanisms may be involved. While cascade-dissolution of precipitate particles cannot be ruled out, dissolution of coarser $M_{23}C_6$ while smaller MC particles survive would not suggest that this is the dominant mechanism. While RIS of chromium seems to be involved in the radiation-induced chromium enrichment of the MC phase [24, 27, 30], it would not consistently explain the dissolution of Cr-rich $M_{23}C_6$ particles. One simple explanation for initial carbide dissolution during irradiation could involve the supersaturation of vacancies and their interaction with carbon atoms in the matrix. Binding of carbon atoms to the excess vacancies produced during irradiation would cause an apparent increase in the solubility of the matrix for carbon, similar to the case proposed recently for austenitic stainless steels [30]. Increased solubility without a change in the instantaneous matrix carbon content would create a transient decrease in carbon activity, which could then cause partial dissolution of pre-existing carbide particles, as is observed. The other aspects of the microstructural evolution in irradiated 9Cr-1MoVNb steel also seem to support this simple mechanism. If depletion of carbon in the matrix below some critical concentration is a necessary condition for Laves phase precipitation, then any increase in the

matrix carbon content due to the carbon atom-vacancy interaction would help to explain why Laves phase does not form during irradiation at 300-500°C. Carbide dissolution is certainly also a contributing factor to the instability of the subgrain boundary structure observed during irradiation, although biased absorption of radiation-produced point defects (ie. interstitials to compensate for the vacancy supersaturation) would ultimately drive continued boundary migration. The inverse temperature dependence of all of these coupled microstructural phenomena is certainly consistent with their dependence on the radiation-produced vacancy supersaturation, as the mechanism implies. In summary, explanations based on changes the residual carbon content of the matrix at 600°C and below, and differences during thermal aging and HFIR irradiation, help to provide a consistent interpretion of microstructural behavior in aged or irradiated 9Cr-1MoVNb steel.

Finally, two more questions should be answered: a.) are the microstructural data presented here consistent with similar data on comparable aged or irradiated martensitic/ferritic steels? b.) do these data or mechanistic insights have implications on the potential for further improvement of 9Cr-1MoVNb steel through alloy development? With regard to stress-free thermal aging, microstructural data on the same two heats of 9Cr-1MoVNb investigated in this work have been presented for 5000h at 593 and 704°C, in conjunction with fatigue studies at the same temperatures [31, 32]. Little change was observed in the as-tempered microstructure at 593°C, but subgrain structure and carbide coarsening was observed at 704°C, consistent with our data. Laves phase forms abundantly during aging of 9Cr-1Mo steels at 500-550°C for 20,000h [13], and its formation along grain and subgrain boundaries has been related to impact embrittlement at lower temperatures [14, 15]. Laves phase

tends to form at higher aging temperatures in modified 12Cr-1Mo steels (600°C in FV 448 (12Cr-1MoVNb) and CRM-12 (12Cr-1MoV) [33], 500-700°C in 12Cr-1MoVW [34]), and even more abundantly in similar steels with more molybdenum (500-600°C in JMFS (10Cr-2MoVNb) [35], 550-650°C in 13Cr-2MoNbV [18]). Laves can even form after only 1h at 730°C in a modified 10Cr-6Mo steel [36]. There is very little aging data at temperatures below 500°C or for times beyond 20,000h. Although some fine VC needles have been observed to form during tempering in CRM-12 [33], our data on the abundant, fine formation of VC needles during aging at lower temperatures appears to be unique.

With regard to irradiated steels, the HFIR data on precipitation in 9Cr-1MoVNb steel irradiated at 300-600°C is also unique. Direct comparison of the same heats of 9 and 12Cr steels irradiated in HFIR and in FFTF (an LMFBR) at 400°C indicates there is little difference in the precipitate microstructure produced in either reactor. Consistent with our results, Laves phase has generally not been observed in most 9-12Cr steels irradiated in LMFBR's below 600°C (EM-10 (9Cr-1Mo) and EM-12 (9Cr-2MoVNb) [10], HT-9 [8, 24, 27], FV 448 [33] or 13Cr-2MoNbV [18]). Laves phase has been observed at 615°C in CRM-12 (with radiation-produced composition modification) [33], and at 650°C in EM-12 [8] during LMFBR irradiation. Only Suzuki et al. [36] found Laves phase below 600°C, in the 10Cr-2MoVNb steel irradiated in HFIR at 500°C to 34 and 57 dpa. In this case, however, the Laves phase composition was highly modified by RIS during irradiation relative to the thermal phase composition. Our observations of instability of the as-tempered microstructure and the radiation-produced compositional modification of the MC phase in 9Cr-1MoVNb irradiated at 300-500°C appear to be new findings.

With regard to further alloy development, new applications of 9Cr-1MoVNb as either a core material in new modular, inherently-safe advanced reactors [37], or as the first-wall material in a MFR, or as boiler tubing in fossil power plants [4] all go beyond those for which this steel was intitially developed and optimized [38, 39]. Furthermore, there is considerable effort in the U.S. [40, 41] and in Japan [42, 43] to develop steels that have reduced long-term radioactivity after exposure in a fusion reactor, but are metallurgically equivalent to conventional 7-9Cr martensitic steels (ie. 9Cr-2WVTa or 8Cr-2WVTa). For non-nuclear, high-temperature applications of 9Cr-1MoVNb, loss of tensile strength, and creep-rupture and fatigue resistance above 550°C appear related to microstructural instability. Laves phase precipitation after long-term exposure at 450-550°C can cause impact embrittlement at lower temperatures and may also lead to structure recovery and softening due to molybdenum depletion. Alloying to further stabilize the carbide precipitate structure (particularly the MC carbides) could improve the high-temperature strength, while both minor compositional variations (lower Si, more C or B [28, 29]) or changes in tempering conditions (higher tempering temperatures and/or shorter times for more residual carbon in the matrix) could reduce Laves phase precipitation during aging. A major concern for the application of 9-12Cr martensitic/ferritic steels in fusion reactors is the increase in their DBTT caused by irradiation at lower temperatures (<450-500°C) [44, 45]. Although such hardening-induced embrittlement may ultimately be related to point-defect and dislocation types of radiation damage in these steels, radiation-induced coarsening of the as-tempered structure does not help; better unirradiated toughness properties are often related to finer rather than coarser grain/subgrain structures. Stability of the as-tempered carbide during irradiation may be

related to alloying changes that either produce more precipitation during tempering or alter the mixture of carbide phases or their compositions (ie, $M_{23}C_6$/MC ratio, VC/NbC ratio, V/Cr ratio in MC phase) for better resistance to dissolution. The microstructural differences observed between aged and neutron-irradiated specimens of 9Cr-1MoVNb steel suggest that different optimization strategies will be needed for nuclear and non-nuclear applications.

CONCLUSIONS

1. Microstructural evolution in 9Cr-1MoVNb steel was significantly different during long-term thermal aging as compared to HFIR irradiation at 600°C and below.

2. During thermal aging for up to 25,000h, the as-tempered microstructure remained stable at 482-593°C, and coarsened at 650 and 704°C.

3. Thermal aging produced abundant amounts of coarse Laves phase and fine VC needles at 482-593°C. The higher silicon heat of steel contained more Laves phase.

4. HFIR irradiation to 37-39 dpa produced "black-dot" dislocation loops only at 300°C, and detectable helium bubbles and voids only at 400°C. No new precipitate phases were observed at 300-600°C.

5. The lath/subgrain boundary structure after irradiation at 300 and 400°C was considerably coarser than that found in as-tempered condition, whereas the subgrain structure after irradiation at 600°C was similar to the as-tempered structure.

6. Some dissolution of $M_{23}C_6$ particles and coarsening of MC particles was observed after irradiation at 300-500°C, but not at 600°C. Substantial

modifications of the MC phase composition (increased Cr, decreased V) were also observed 300-500°C.

Acknowledgments

Research sponsored by the Office of Fusion Energy, U.S. Department of Energy, under Contract DE-AC05-84OR21400, with Martin Marietta Energy Systems, Inc. We would like to thank Dr. V. Sikka at ORNL for supply the thermally aged steel specimens. We would like to thank N. Rouse for expert thinning of the HFIR irradiated TEM specimens, and W. Jones for thinning and preparing replicas on the aged steel specimens.

REFERENCES

1. G.W. Cunningham, P. Patriarca and E.E. Hoffman, *Ferritic Steels for High-Temperature Applications*, A.K. Khare, Ed., American Society for Metals, Metals Park, OH, 1983, p. 3.

2. H. Haneda, F. Masuyama, S. Kaneko and T. Toyoda, *Advances in Materials Technology for Fossil Power Plants*, R. Viswanathan and R.I. Jaffee, ASM International, Metals Park, OH, 1987, p. 231.

3. Pelabon, J. and Pellicani, F., *Advances in Materials Technology for Fossil Power Plants*, R. Viswanathan and R.I. Jaffee, ASM International, Metals Park, OH, 1987, p. 243.

4. Jaske, C.E. and Swindeman, R.W., *Advances in Materials Technology for Fossil Power Plants*, R. Viswanathan and R.I. Jaffee, ASM International, Metals Park, OH, 1987, p. 251.

5. Bodine, G.C. and McDonald, R.E., *Ferritic Steels for High-Temperature Applications*, A.K. Khare, Ed., American Society for Metals, Metals Park, OH, 1983, p. 9.

6. Sikka, V.K., Ward, C.T. and Thomas, K.C., *Ferritic Steels for High-Temperature Applications*, A.K. Khare, Ed., American Society for Metals, Metals Park, OH, 1983, p. 65.

7. Bagley, K.Q., Little, E.A., Levy, V., Alamo, A., Ehrlich, K., Anderko, K., and Calzabini, A., *Materials For Nuclear Reactor Core Applications*, Bristol Meeting, Oct. 1987, Vol. 2, British Nuclear Energy Society, London, 1988, p. 37.

8. Gelles, D.S. and Thomas, L.E., *Proceedings of a Topical Conference on Ferritic Alloys for Use in Nuclear Energy Technologies*, J.W. Davis and D.J. Michel, Eds., The Metallurgical Society of American Institute of Mining, Metallurgical and Petroleum Engineers, New York, 1984, p. 559.

9. Gelles, D.S., *Journal of Nuclear Materials*, Vol. 148, 1987, p. 136.

10. Gilbon, D., Seran, J., Cauvin, R., Fissolo, A., Alamo, A., Le Naour, F. and Levy, V., *Effects of Radiation on Materials: 14th International Symposium, Volume I, ASTM STP 1046*, N.H. Packan, R.E. Stoller and S. Kumar, Eds., American Society for Testing and Materials, Philadelphia, 1989, p. 5.

11. Klueh, R.L. and Tanaka, M.P., *Journal of Metals*, Vol. 37, Oct. 1985, p. 16.

12. Bloom, E.E. and Smith, D.L., *Proceedings of Conference on Materials for Future Energy Systems*, held in Washington, D.C. May 1-3, 1984, American Society for Metals, Metals Park, OH, 1985, p. 253.

13. Titchmarsh, J.M., Wall, M. and Edwards, B.C., *Analytical Electron Microscopy*, D.B. Williams and D.C. Joy, Eds., San Francisco Press, San Francisco, CA, 1984, p. 247.

14. Hudson, J.A., Druce, S.G., Gage, G., and Wall, M., *Journal of Theoretical and Applied Fracture Mechanics*, Vol. 10, 1988, p. 123.

15. Wall, M., *Temper Embrittlement in 9% Chromium Steel*, Ph. D. thesis submitted to University of London, AEA Technology Harwell - AERE-R12812, Harwell Laboratory, Oxfordshire, England, August 1985.

16. Hu, W.L. and Gelles. D.S., *Influence of Radiation on Materials Properties: 13th International Symposium (Part II), ASTM STP 956*, F.A. Garner, C.H. Henager and N. Igata, Eds., American Society for Testing and Materials, Phildelphia, PA, 1987, p. 83.

17. Vitek, J.M., Corwin, W.R., Klueh, R.L. and Hawthorne, J.R., *Journal of Nuclear Materials*, Vols. 141-143, 1986, p. 948.

18. Agueev, V.S., Bykov, V.N., Dvoryashin, A.M., Golovanov, E.A., Medvedeva, E.A., Romaneev, V.V., Shamardin, V.K., and Vorobiev, A.N., *Effects of Radiation on Materials: 14th International Symposium, Volume I, ASTM STP 1046*, N.H. Packan, R.E. Stoller and S. Kumar, Eds., American Society for Testing and Materials, Philadelphia, 1989, p. 98.

19. Klueh, R.L. and Maziasz, P.J., *Effects of Radiation on Materials: 14th International Symposium, Volume I, ASTM STP 1046*, N.H. Packan, R.E. Stoller and S. Kumar, Eds., American Society for Testing and Materials, Philadelphia, 1989, p. 246.

20. Klueh, R.L. and Alexander, D.J., in the Proceedings of the 4th International Conference on Fusion Reactor Materials (ICFRM-4), Tokyo, Japan, Dec. 1-4, 1989; to be published in *Journal of Nuclear Materials* in 1990.

21. Zaluzec, N.J., *Introduction to Analytical Electron Microscopy*, J.J. Hren, J.I. Goldstein, and D.C. Joy, Eds., Plenum Press, New York, 1979, p. 121.

22. Maziasz, P.J. and Odette, G.R., *Proceedings of the 41st Annual EMSA Meeting*, G.W. Bailey, Ed., San Francisco Press, San Francisco, 1983, p. 198.

23. Kenik, E.A. and Maziasz, P.J., *Analytical Electron Microscopy - 1984*, D.B. Williams and D.C. Joy, Eds., San Francisco Press, San Francisco, 1984, p. 231.

24. Maziasz, P.J. and Klueh, R.L., *Effects of Radiation on Materials: 14th International Symposium, Volume I, ASTM STP 1046*, N.H. Packan, R.E. Stoller and A.S. Kumar, Eds., American Society for Testing and Materials, Philadelphia, 1989, p. 35.

25. Vitek, J.M. and Klueh, R.L., *Proceedings of a Topical Conference on Ferritic Alloys for Use in Nuclear Energy Technologies*, J.W. Davis and D.J. Michel, Eds., The Metallurgical Society of American Institute of Mining, Metallurgical and Petroleum Engineers, New York, 1984, p. 551.

26. Maziasz, P.J. and Sikka, V.K., *ADIP Semiannu. Prog. Rept. DOE/ER-0045/15 ending Sept. 30, 1985*, U.S. Dept. of Energy, (Feb.,1986) p. 102.

27. Maziasz, P.J., Klueh, R.L. and Vitek, J.M., *Journal of Nuclear Materials*, Vol. 141-143, 1986, p. 929.

28. Maziasz, P.J., *MiCon '86: Optimization of Processing, Properties and Service Performance Through Microstructural Control, ASTM STP 979*, American Society for Testing and Materials, Philadelphia PA, 1988, p. 116.

29. Maziasz, *Journal of Minerals, Metals and Materials (JOM)*, Vol. 41, no. 7, 1989, p. 14.

30. Maziasz, P.J., *Journal of Nuclear Materials*, Vol. 169, 1990, p. 95.

31. Matsuoka, S., Kim, S., and Weertman, J.R., *Proceedings of a Topical Conference on Ferritic Alloys for Use in Nuclear Energy Technologies*, J.W. Davis and D.J. Michel, Eds., The Metallurgical Society of American Institute of Mining, Metallurgical and Petroleum Engineers, New York, 1984, p. 507.

32. Kim, S. and Weertman, J.R., *Metallurgical Transactions A*, Vol. 19A, 1988, p. 999.

33. Stoter, L.P. and Little, E.A., *Advances in the Physical Metallurgy and Applications of Steels*, The Metals Society, London, 1981, p. 369.

34. Chen, P.S. and Wilcox, R.C., *Effects of Radiation on Materials: 14th International Symposium, Volume I, ASTM STP 1046*, N.H. Packan, R.E. Stoller and A.S. Kumar, Eds., American Society for Testing and Materials, Philadelphia, 1989, p. 114.

35. Suzuki, M., Hishinuma, A., Maziasz, P.J. and Sawai, T., *Journal of Nuclear Materials*, Vol. 170, 1990, p. 270.

36. Farrell, K. and Lee, E.H., *Scripta Metallurgica*, Vol. 17, 1983, p. 791.

37. "PRISM Makes Progress," *Nuclear Engineering International*, September, 1988, p. 32.

38. Patriarca, P. *Proceedings of a Topical Conference on Ferritic Alloys for Use in Nuclear Energy Technologies*, J.W. Davis and D.J. Michel, Eds., The Metallurgical Society of American Institute of Mining, Metallurgical and Petroleum Engineers, New York, 1984, p 107.

39. Sikka, V.K., Cowgill, M.G. and Roberts, B.W., *Proceedings of a Topical Conference on Ferritic Alloys for Use in Nuclear Energy Technologies*, J.W. Davis and D.J. Michel, Eds., The Metallurgical Society of American Institute of Mining, Metallurgical and Petroleum Engineers, New York, 1984, p. 413.

40. Klueh, R.L. and Maziasz, P.J., *Journal of Nuclear Materials*, Vol. 155-157 (1988) p. 602.

41. Gelles, D.S., *Reduced Activation Materials for Fusion Reactors ASTM STP 1047*, R.L. Klueh, D.S. Gelles, M. Okada and N.H. Packan, Eds., American Society for Testing and Materials, Philadelphia PA, 1990, p. 113.

42. Tamura, M., Hayakawa, H., Yoshitake, A., Hishinuma, A. and Kondo, T., *Journal of Nuclear Materials*, Vol. 155-157 (1988) p. 620.

43. Abe, F., Noda, T., Araki, H., and Okada, M., *Reduced Activation Materials for Fusion Reactors ASTM STP 1047*, R.L. Klueh, D.S. Gelles, M. Okada and N.H. Packan, Eds., American Society for Testing and Materials, Philadelphia PA, 1990, p. 130.

44. Vitek, J.M., Corwin, W.R., Klueh, R.L., and Hawthorne, J.R., *Journal of Nuclear Materials*, Vols. 141-143, 1986, p. 948.

45. Klueh, R.L. and Maziasz, P.J., *Effects of Radiation on Materials: 14th International Symposium, Volume I, ASTM STP 1046*, N.H. Packan, R.E. Stoller and A.S. Kumar, Eds., American Society for Testing and Materials, Philadelphia, 1989, p. 246.

FIGURE CAPTIONS

1. The microstructure produced in 9Cr-1MoVNb steel (heat 30176) after tempering for 1h at 760°C. a.) TEM of a thin-foil specimen, and b.) TEM of precipitates extracted onto a carbon replica film (with histograms of phase compositions from quantitative XEDS analysis).

2. TEM of the lath/subgrain boundary and matrix dislocation structures of 9Cr-1MoVNb (heat 30176) steel in a.) the as-tempered condition and after aging for 25,000h at b.) 538°C and c.) 650°C.

3. TEM of the lath/subgrain structure of 9Cr-1MoVNb (heat 30176) steel after aging for 25,000h at 704°C.

4. Plots of a.) weight fraction (wt.%) of precipitate extracted from bulk specimens and b.) the molybdenum concentration from quantitative broad-beam XEDS analysis of precipitates on extraction replicas, both from specimens of the two heats of 9Cr-1MoVNb steel after various aging treatments.

5. Precipitation of Laves phase as films along grain boundaries in 9Cr-1MoVNb (heat 30394) steel aged for 25,000h at 538°C, as shown with TEM in a.) bright-field, b.) precipitate dark-field and c.) selected area diffraction (SAD) modes.

6. Comparison of differences in the amount and distribution of Laves phase in different heats of 9Cr-1MoVNb steel during aging at 538°C for 25,000h. a.) heat 30176 (0.1 wt.% Si) and b.) heat 30394 (0.4 wt.% Si). Both specimens are extraction replicas.

7. Fine MC precipitation formed during aging of 9Cr-1MoVNb steel at 538°C for 25,000h. a.) bright-field, b.) precipitate dark-field and c.) SAD TEM analysis from a thin-foil specimen of heat 30176 and d.) TEM of an extraction replica specimen of heat 30394.

8. TEM of the lath/subgrain boundary and matrix dislocation structures of 9Cr-1MoVNb (heat XA 3590) steel a.) and b.) as-tempered, and c.) and d.) after HFIR irradiation at 300°C to about 37 dpa, at both lower (a,c) and higher (b,d) magnifications.

9. TEM of larger voids and finer helium bubbles formed in 9Cr-1MoVNb (heat XA 3590) steel after HFIR irradiation at 400°C to about 37 dpa, at lower (a) and higher (b) magnifications.

10. TEM the lath/subgrain boundary, dislocation and precipitate structures of 9Cr-1MoVNb (heat XA 3590) steel after HFIR irradiation at 500°C to about 39 dpa.

11. TEM the lath/subgrain boundary, dislocation and precipitate structures of 9Cr-1MoVNb (heat XA 3590) steel after HFIR irradiation at 600°C to about 39 dpa.

12. Histograms of MC phase composition from quantitative XEDS analysis of precipitate particles on extraction replicas from 9Cr-1MoVNb (heat XA 3590) steel in the as-tempered condition and after HFIR irradiation at 400°C to about 37 dpa.

13. A plot of the average chromium and vanadium concentrations of MC particles as functions of exposure temperature, obtained from quantitative XEDS analysis of extraction replicas made from 9Cr-1MoVNb (heat XA 3590) steel specimens which had been thermally aged or irradiated in HFIR.

Table 1. Compositions of Two Commercial Heats of 9Cr-1MoVNb

Heat Designation	Alloy Composition,[a] wt %											
	Cr	Mo	V	Nb	Mn	Ni	Si	C	Cu	W	P	N
30176	8.6	0.9	0.21	0.072	0.37	0.09	0.11	0.081	0.04	<0.01	0.01	0.0055
30394	8.6	1.0	0.20	0.073	0.46	0.09	0.4	0.084	0.04	0.05	0.01	0.053
XA 3590[b]	8.6	1.0	0.21	0.063	0.36	0.1	0.08	0.09		0.01		0.05

[a]Balance iron. [b]0.002 Ti.

Table 2. Precipitatation Data on Thermally Aged 9Cr-1MoVNb Specimens

Specimen Designation	Aging Conditions: Temperature (°C)	Aging Conditions: Time (h)	Bulk Precipitate Extraction (wt %)	Phases Observed on Extraction Replicas via XEDS[a]
			Heat 30176 (0.1 wt % Si)	
T-20	As-tempered (1 h @ 760°C)		1.713	$M_{23}C_6$ + VC + NbC
24047	482	25,000	2.087	$M_{23}C_6$ + Laves + VC + NbC + $Cr_2(X)$?
T-214	538	10,000	2.027	$M_{23}C_6$ + Laves + VC
T-344	538	25,000	2.358	$M_{23}C_6$ + Laves + VC + some fine Fe-Cr phase
T-362	593	25,000	2.247	$M_{23}C_6$ + Laves + VC + NbC
T-246	650	10,000	1.748	$M_{23}C_6$ + VC + NbC
T-378	650	25,000	1.810	$M_{23}C_6$ + VC + NbC
T-394	704	25,000	1.786	$M_{23}C_6$ + VC +NbC
			Heat 30394 (0.4 wt % Si)	
T-19	As-tempered (1 h @ 760°C)		1.833	$M_{23}C_6$ + VC + NbC
23985	482	25,000	3.137	$M_{23}C_6$ + Laves + VC + NbC
T-616	538	25,000	3.183	$M_{23}C_6$ + Laves + VC + NbC + some fine Fe-Cr phase
T-313	650	10,000	1.802	$M_{23}C_6$ + VC + NbC
T-584	650	25,000	2.729	$M_{23}C_6$ + Laves + VC + NbC

[a]Phase identified by characteristic spectra from individual particle analysis; relative phase fraction determined from broad-beam XEDS of many particles. Order represents decreasing phase fraction.

Table 3. Broad-Beam Compositional Averaging via XEDS of Precipitates Extracted onto Replicas from Aged 9Cr-1MoVNb Steel

Aging Conditions		Phases	Alloy Composition,[a] at. %									
Temperature (°C)	Time (h)		Si	P	Ti	V	Cr	Mn	Fe	Ni	Nb	Mo
		Heat 30176										
As-tempered		$M_{23}C_6$ + VC + NbC	4.0	0.5	0.1	8.3	54.5	0.2	25	0.2	3.0	4.5[2][b]
482	25,000	$M_{23}C_6$ + Laves + VC + NbC + $Cr_2(X)$?	0.5	0.9	0.1	8.2	54.2	0.1	24.8	0.1	4.1	7.0[2]
538	10,000	$M_{23}C_6$ + Laves + VC	2.7	2.3	0.1	7.0	48.0	1.5	27.4	0.4	1.8	9.0[2]
538	25,000	$M_{23}C_6$ + Laves + VC + fine Fe-Cr phase	2.4	1.3	0.1	6.6	45.6	0.6	29.3	0.1	1.8	12.3[2]
593	25,000	$M_{23}C_6$ + Laves + VC + NbC	3.7	2.1	0.1	5.5	44.7	0.5	27.5	0.1	2.1	13.7[2]
650	10,000	$M_{23}C_6$ + VC + NbC	4.5	1.4	0.2	6.6	63.2	1.2	17.0	0.3	2.3	4.4[2]
650	25,000	$M_{23}C_6$ + VC + NbC	4.3	0.7	0.1	8.8	61.5	0.4	16.1	0.2	2.9	5.3[2]
704	25,000	$M_{23}C_6$ + VC +NbC	1.5		0.1	11.0	59.2	1.4	16.2	0.6	5.6	4.4[3]
		Heat 30394										
As-tempered		$M_{23}C_6$ + VC + NbC	2.8	1.3		7.5	56.4	1.3	24.5	0.1	1.3	4.5[2][b]
482	25,000	$M_{23}C_6$ + Laves + VC + NbC	3.8	1.2	0.1	9.4	39.6	0.6	27.4	0.2	3.9	13.8[2]
538	25,000	$M_{23}C_6$ + Laves + VC + NbC + some fine Fe-Cr	5.6	2.0	0.1	4.9	39.5	0.8	30.8		1.3	15.0[2]
650	10,000	$M_{23}C_6$ + VC + NbC	1.3	1.6	0.2	8.5	59.7	1.3	17.9	0.4	3.8	5.4[2]
650	25,000	$M_{23}C_6$ + Laves + VC + NbC	5.5	1.6	0.1	4.7	41.6	0.6	28.9	0.1	1.3	15.7[2]

[a]Normalized, averaged composition for elements heavier than aluminum.

[b]The number of spectra obtained from different areas of the replica for the average broad-beam composition.

Table 4. XEDS Composition of the Laves Phase Extracted on Replicas from Aged 9Cr-1MoVNb Steel

Aging Conditions		Comments[a]	Composition[b] (at. %)									
Temperature (°C)	Time (h)		Si	P	Ti	V	Cr	Mn	Fe	Ni	Nb	Mo
					Heat 30176							
482	25,000	Large[2]	2.4	4.6	0.1	0.1	17.8	1.0	39.0	0.3	0.2	34.5
538	10,000	Large[3]	7.6	5.2	0.1	0.4	12.8	1.4	43.4	0.4	0.3	28.3
538	25,000	Large[3]	7.1	2.8	0.2	0.6	13.2	0.9	43.0	0.2	0.3	31.8
593	25,000	Large[2]	8.2	3.4	0.2	0.1	9.6	0.6	45.1	0.2	0.3	32.3
					Heat 30394							
538	25,000	Large[3]	13.4	3.6		2.2	13.5	0.8	38.3	0.1	0.5	27.0
650	25,000	Large[4]	11.5	3.2	0.1	0.3	12.8	0.6	42.6	0.7	0.7	28.1

[a]Large particles are usually greater than 200 nm in size (numbers in brackets indicate the number of individual particle spectra analyzed).

[b]Normalized, averaged composition for elements heavier than aluminum.

Table 5. XEDS Composition of MC Individual Particles Extracted on Replicas from Aged 9Cr-1MoVNb Steel

Aging Conditions		Phases and Comments[a]	Composition[b] (at. %)									
Temperature (°C)	Time (h)		Si	P	Ti	V	Cr	Mn	Fe	Ni	Nb	Mo
		Heat 30176										
As-tempered		Small VC [5]	1.4	0.1	0.1	74.0	16.9		0.5		6.3	0.6
		Larger NbC[1]				12.2	2.2		0.4		84.7	0.5
		Small NbC[2]				15.3	3.3		0.5		80.2	0.6
482	25,000	g.b.[c] VC [3]	0.5	0.8	0.1	65.8	19.3		3.6		7.1	2.7
		Larger matrix VC[1]	1.2	0.6		68.2	16.1		4.6	0.1	8.7	0.7
		Very fine VC [3]	5.4	1.5	0.2	59.0	23.6		2.8	0.1	3.9	3.5
		Larger matrix NbC[1]		5.9		16.4	3.4	0.1	0.6	0.1	72.5	0.8
		Larger matrix MC[1]		3.0	0.3	51.6	12.8		1.1	0.1	26.9	4.2
538	10,000	Small VC[5]	0.5	0.5	0.2	68.0	20.8		2.3	4.6	3.7	3.6
538	25,000	Larger VC[4]		0.6	0.1	68.4	22.4		3.1	0.1	4.3	1.0
		Very fine VC[1]	8.1	0.2		52.5	23.1		9.3	0.1	2.7	4.0
593	25,000	Larger VC[2]	3.3	0.8	0.2	72.0	12.5	0.1	0.7		9.8	0.6
		Small VC[1]	3.6	1.0	0.2	73.8	14.1	0.1	0.5	0.1	5.8	0.8
		Larger NbC[1]	1.8	1.5	0.3	14.8	3.0	0.2	0.6	0.1	77.6	0.3
650	10,000	Small VC [3]	2.5	0.8		75.8	14.6		0.3		5.1	0.8
650	25,000	Larger VC[5]	1.3	1.1	0.1	67.2	16.2		1.3		12.1	0.7
		Small VC[9]	2.8	0.8	0.1	75.1	13.5		0.6		6.6	0.6
		Small NbC[2]		6.5	0.1	14.0	2.7		0.4		76.6	0.7
704	25,000	Larger VC [2]	1.1		0.7	66.4	6.6		0.7	0.5	23.6	0.2
		Small VC[4]	0.5		0.7	70.7	12.1		0.9	0.6	14.0	0.6
		Larger MC[3]	1.7		0.5	48.5	5.5		0.5	0.7	42.3	0.3
		Small MC[3]	1.8		0.4	49.2	5.2		0.5	0.6	41.8	0.6
		Larger NbC[1]	3.6		0.4	8.1	1.7		0.6	0.9	84.0	0.4
		Heat 30394										
As-tempered		Small VC[1]	1.2	2.1	0.9	75.3	14.2		0.1		5.6	0.7
		Small NbC[1]	6.4	2.0		15.2	3.0		0.5		71.6	1.4
538	25,000	Small VC[6]		1.0		77.6	15.3				5.5	0.3
650	10,000	Larger VC[2]	1.4	2.8	0.1	71.2	8.9		0.4		14.4	0.9
		Small VC[2]	3.1	3.4	0.1	64.2	10.0		0.7	0.1	16.5	1.9
650	25,000	Small VC[5]	3.2	1.8	0.1	70.3	15.0	0.1	0.9		7.5	0.9

[a]Larger particles are greater than ~50 to 60 nm in size, small particles are less than ~30 to 40 nm in size, and very fine particles are usually rods, ~5-nm-thick, 40- to 100-nm-long (numbers in brackets indicate the number of individual particle spectra analyzed).

[b]Normalized, averaged composition for elements heavier than aluminum. [c]g.b. = grain boundary.

Table 6. Broad-Beam Compositional Averaging via XEDS of Precipitates Extracted onto Replicas from HFIR-Irradiated 9Cr-1MoVNb Steel

Aging Conditions		Phases	Composition[a] (at. %)								
Temperature (°C)	Dose (dpa)		Si	Ti	V	Cr	Mn	Fe	Ni	Nb	Mo
As-tempered		$M_{23}C_6$ + MC[2][b]	0.9	0.4	9.7	53.3	0.1	26.5	0.4	3.4	4.8
300	36.5	$M_{23}C_6$ + MC[3]	2.0	0.1	10.5	53.8	0.6	25.6	0.1	2.6	3.6
400	36.5	$M_{23}C_6$ + MC[5]	1.9	0.06	5.7	61.7	0.7	23.2	0.5	2.6	3.6
500	38.5	$M_{23}C_6$ + MC[2]	2.8	0.3	5.8	58.6	0.1	22.1	2.0	3.2	4.6
600	38.5	$M_{23}C_6$ + MC[3]	1.4	0.3	6.9	60.7	3.9	22.6	0.1	1.1	3.1

[a]Normalized, averaged composition for elements heavier than aluminum.

[b]The number of separate spectra obtained from different areas of the replica for the average broad-beam composition.

[c]None detected.

Table 7. XEDS Composition of Individual MC Particles Extracted onto Replicas from HFIR-Irradiated 9Cr-1MoVNb Steel

Aging Conditions		Comments[a]	Composition[a] (at. %)							
Temperature (°C)	Dose (dpa)		Si	Ti	V	Cr	Fe	Ni	Nb	Mo
As-Tempered		Small[b] VC[6][c]	1.6	0.6	64.0	16.6	1.6	nd[d]	1.3	5.2
		Small NbC[2]	2.3	2.3	33.5	9.2	1.1	0.1	50.5	1.3
300	36.5	Small VC[4]	1.5	0.4	42.3	36.8	8.9	0.08	8.0	1.0
		Small NbC[3]	2.2	0.2	11.4	17.2	10.0	0.3	53.9	3.1
400	36.5	Small VC[9]	3.2	0.5	35.0	46.5	5.5	0.4	7.4	1.4
		Small NbC[2]	0.4	1.2	8.8	34.2	4.5	0.8	46.1	3.5
500	38.5	Small VC[9]	2.5	0.7	33.9	41.9	10.0	1.0	7.5	1.5
		Small NbC[2]	2.6	1.1	9.8	27.5	7.4	0.8	46.3	3.1
600	38.5	Small MC[8]	2.1	0.4	53.6	27.9	7.0	nd[c]	7.3	1.4

[a]Normalized, averaged composition for elements heavier than aluminum.

[b]Particles are less than 50 to 60 nm in diameter.

[c]The number of separate spectra obtained from different particles for the average phase composition.

[d]None detected.

ORNL-PHOTO 5044-90

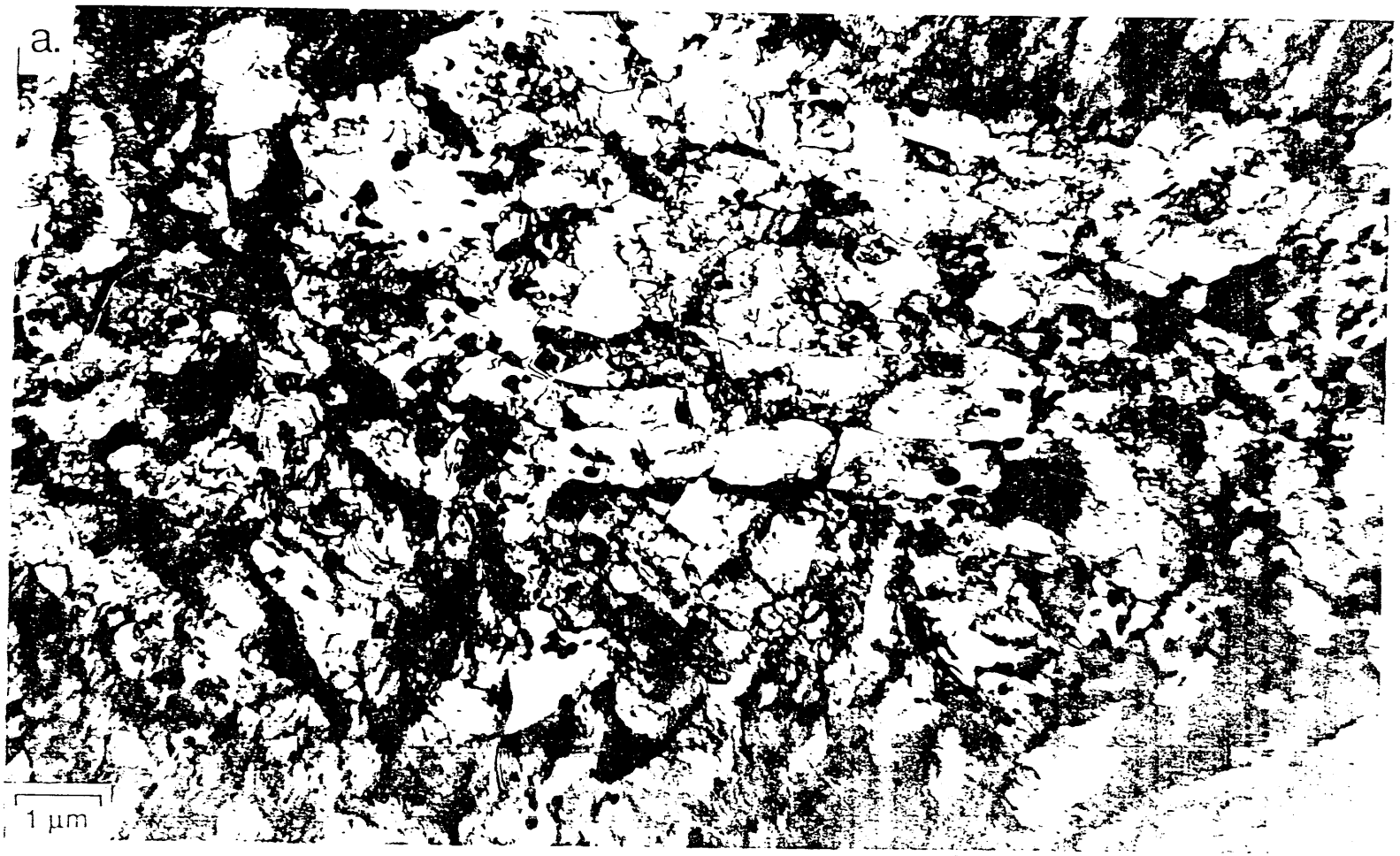

Fig 1

Fig 1 cont.

ORNL-PHOTO 5045-90

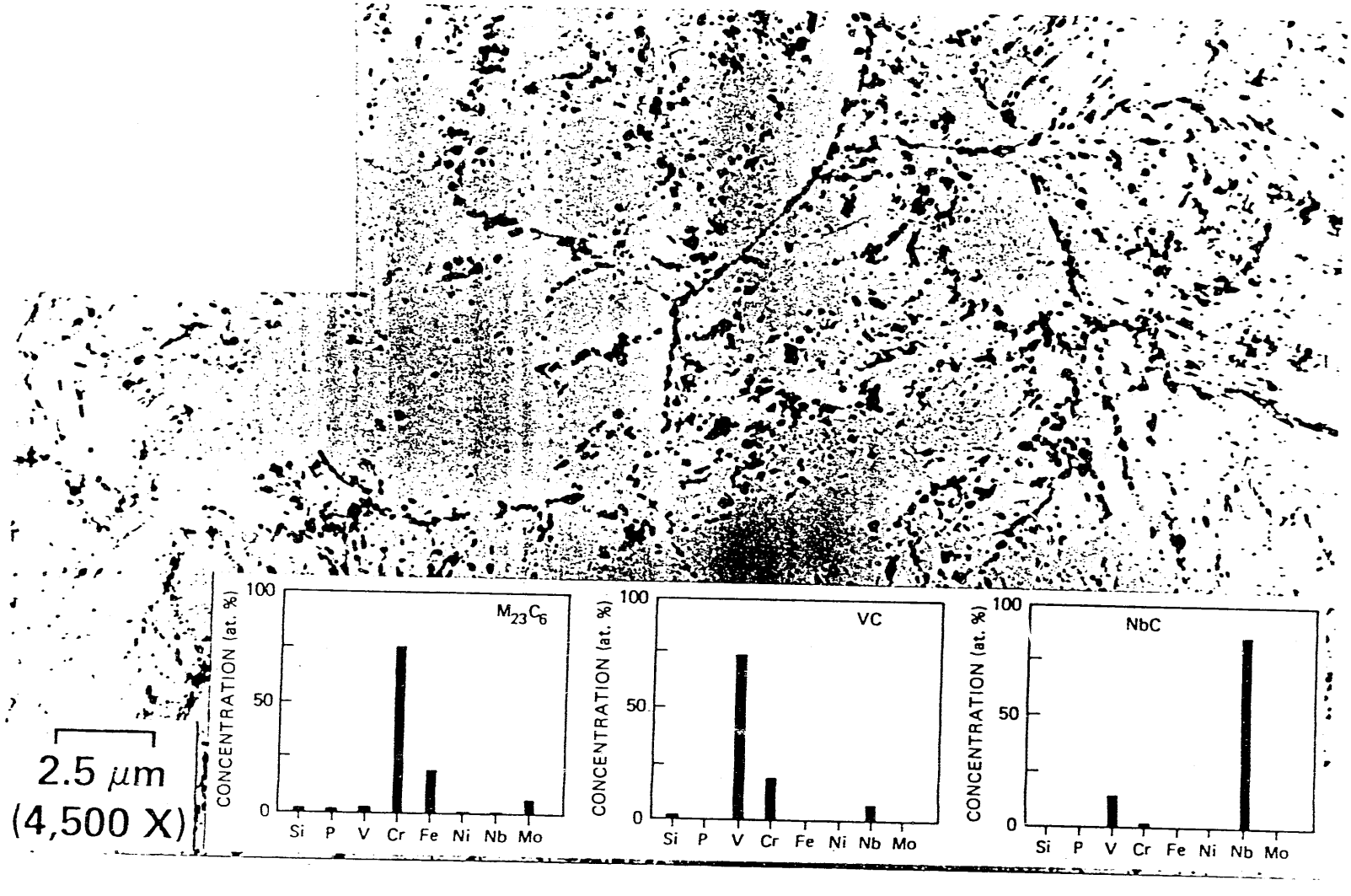

ORNL-DWG 90M-12157R

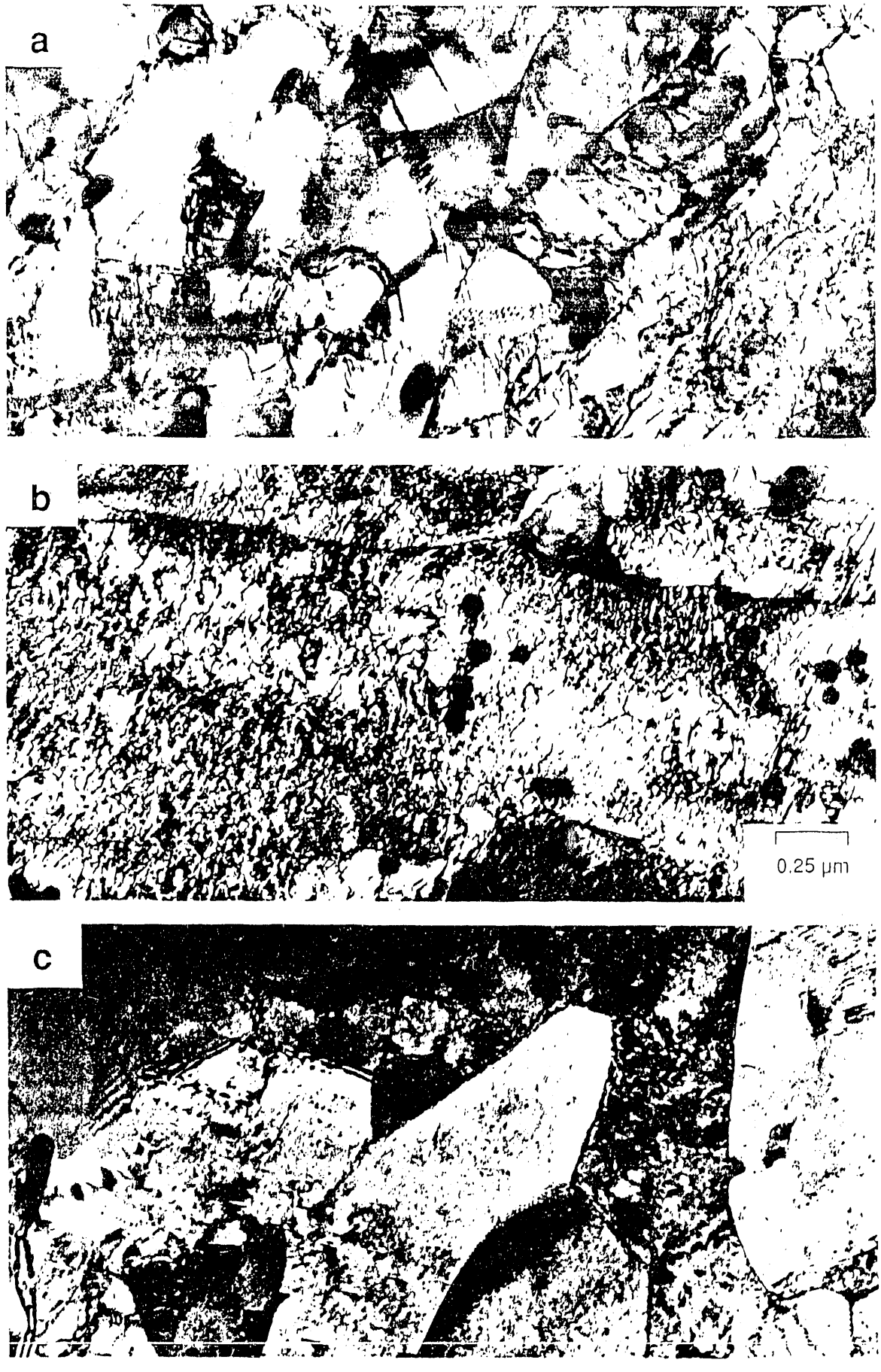

Fig 2

ORNL-PHOTO 5039-90

Fig. 3

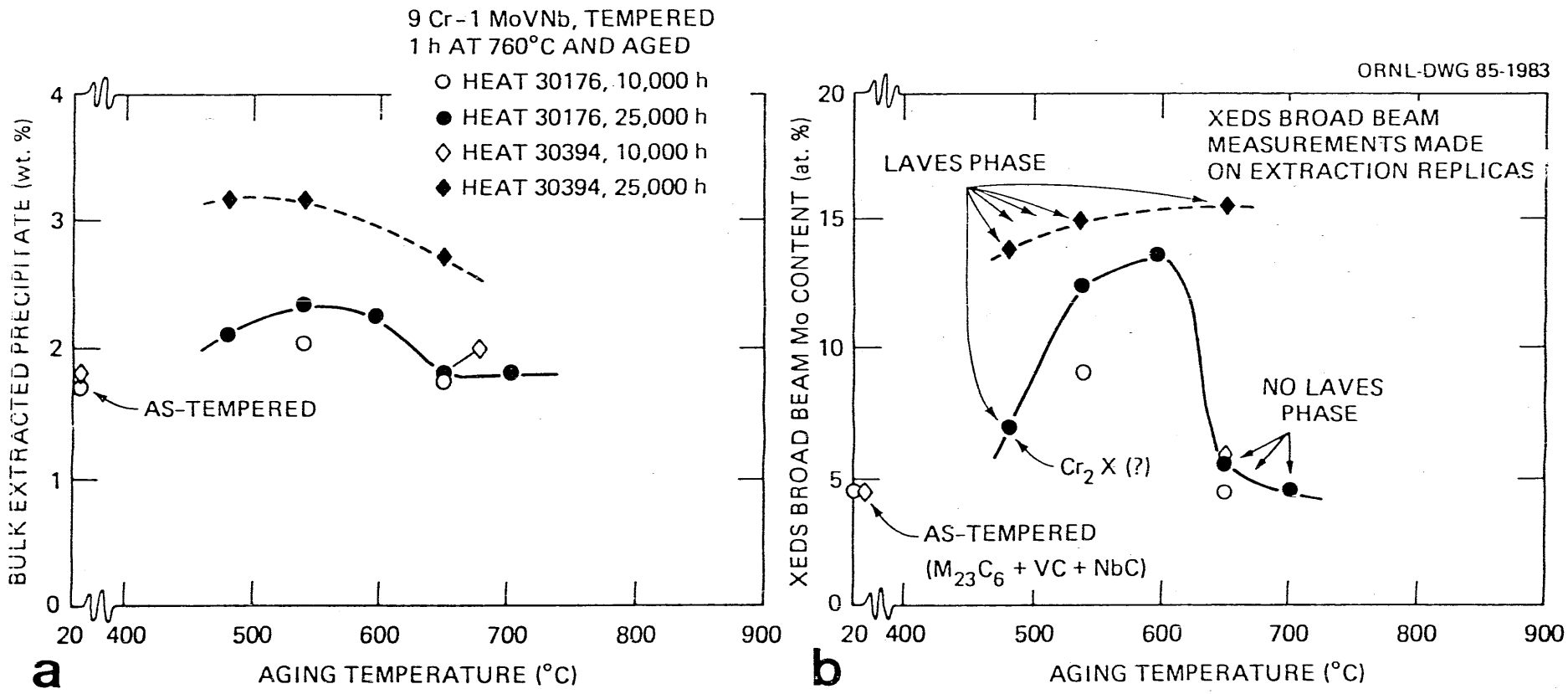
9 Cr-1 MoVNb, TEMPERED
1 h AT 760°C AND AGED
HEAT 30176, 10,000 h
HEAT 30176, 25,000 h
HEAT 30394, 10,000 h
HEAT 30394, 25,000 h
BULK EXTRACTED PRECIPITATE (wt. %)
AS-TEMPERED
AGING TEMPERATURE (°C)
a
ORNL-DWG 85-1983
XEDS BROAD BEAM MEASUREMENTS MADE ON EXTRACTION REPLICAS
LAVES PHASE
NO LAVES PHASE
Cr_2X (?)
AS-TEMPERED
($M_{23}C_6$ + VC + NbC)
XEDS BROAD BEAM Mo CONTENT (at. %)
AGING TEMPERATURE (°C)
b

Fig. 4


a.
GRAIN BOUNDRY
b.
LAVES PHASE FILMS
0.25 μm
c.
(220)α
(200)α
(01.3)LAVES

Fig. 5

ORNL-PHOTO 5348-90

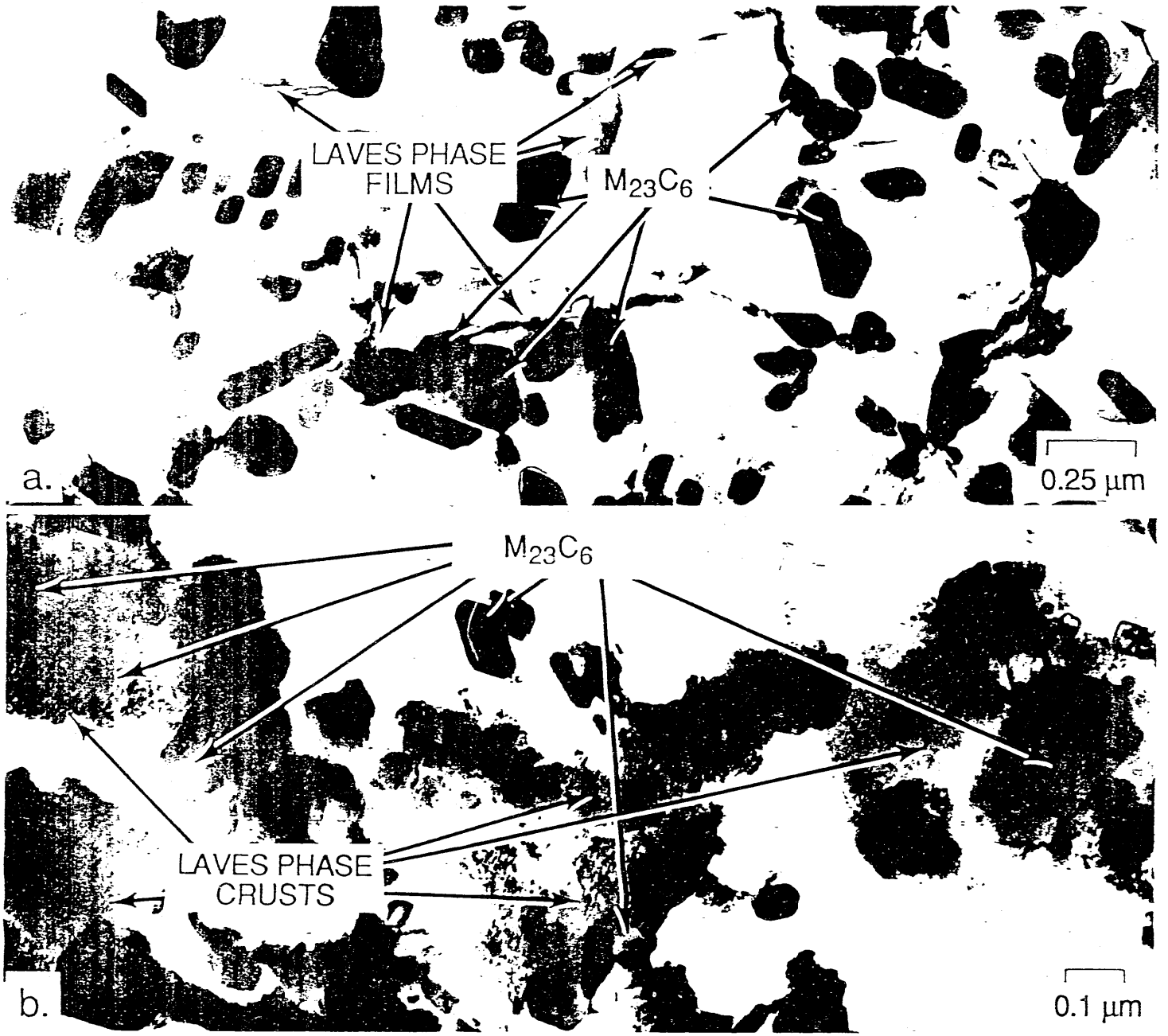

Fig. 6

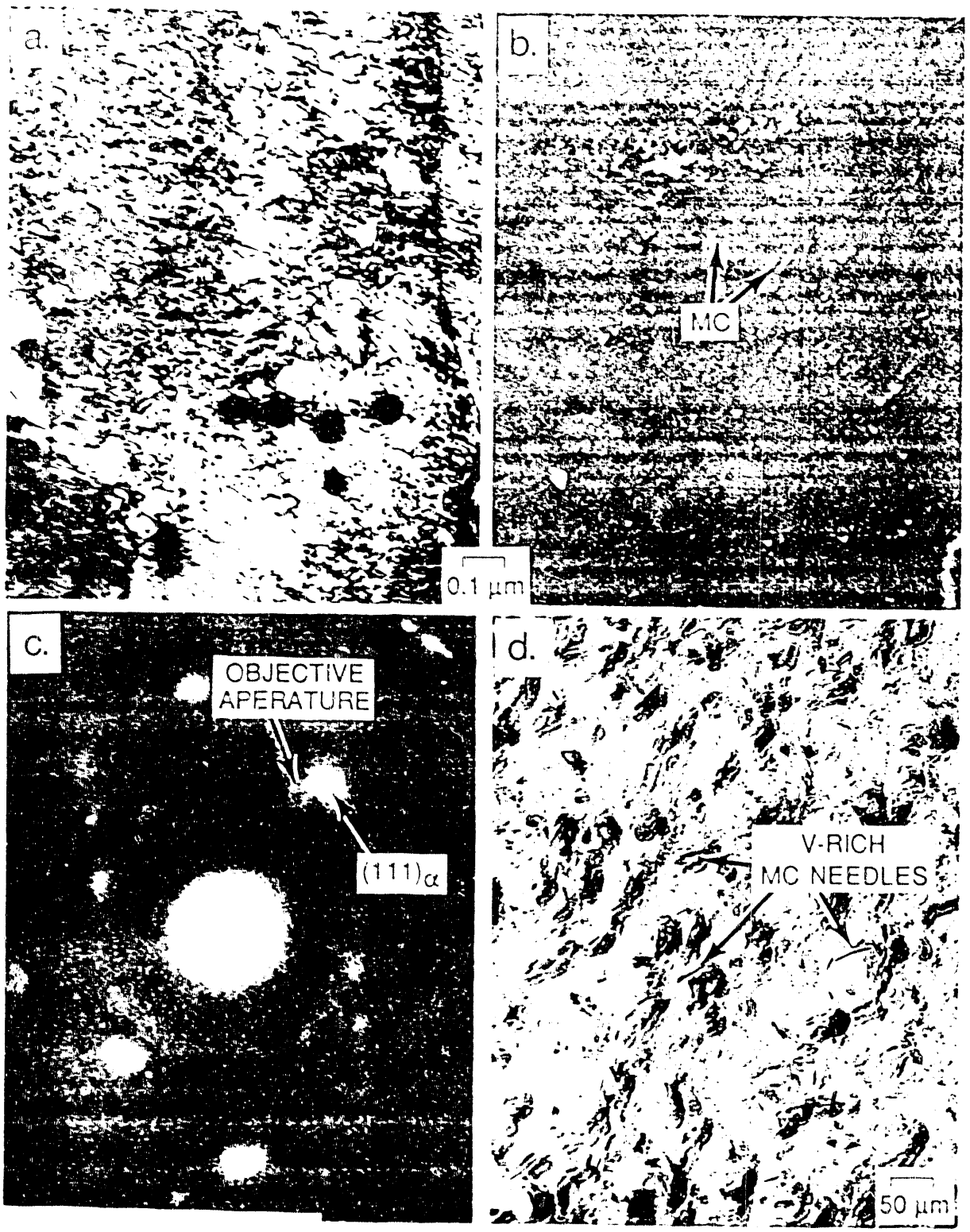
a.
0.1 μm
b.
MC
c.
OBJECTIVE
APERATURE
(111)α
d.
V-RICH
MC NEEDLES
50 μm

Fig. 7

ORNL-DWG 90M-12158R

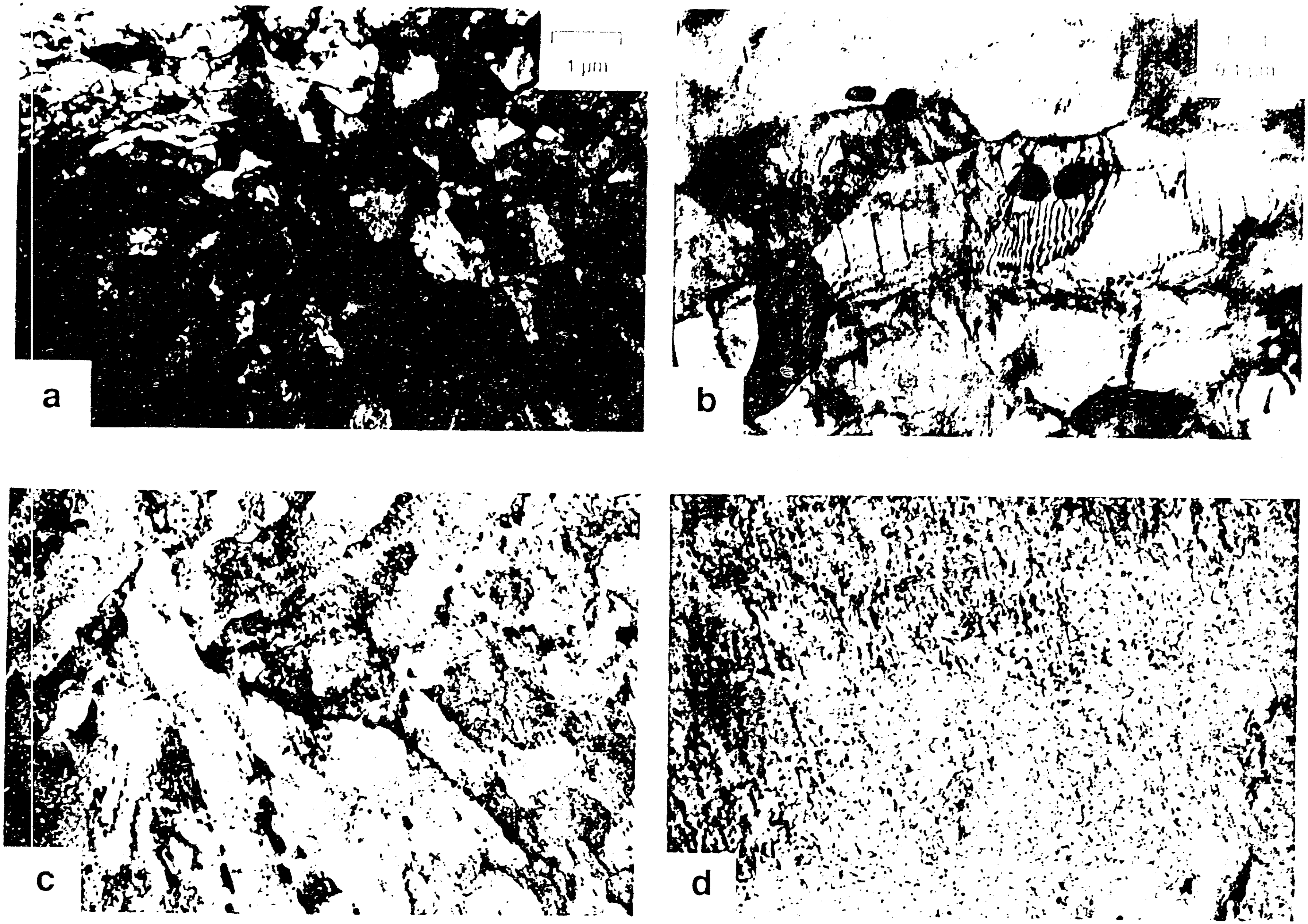

Fig.

ORNL-PHOTO 5043-90

Fig. 9

ORNL-PHOTO 5046-90

Fig. 16

ORNL-PHOTO 5042-90

Fig. 11

ToC 24

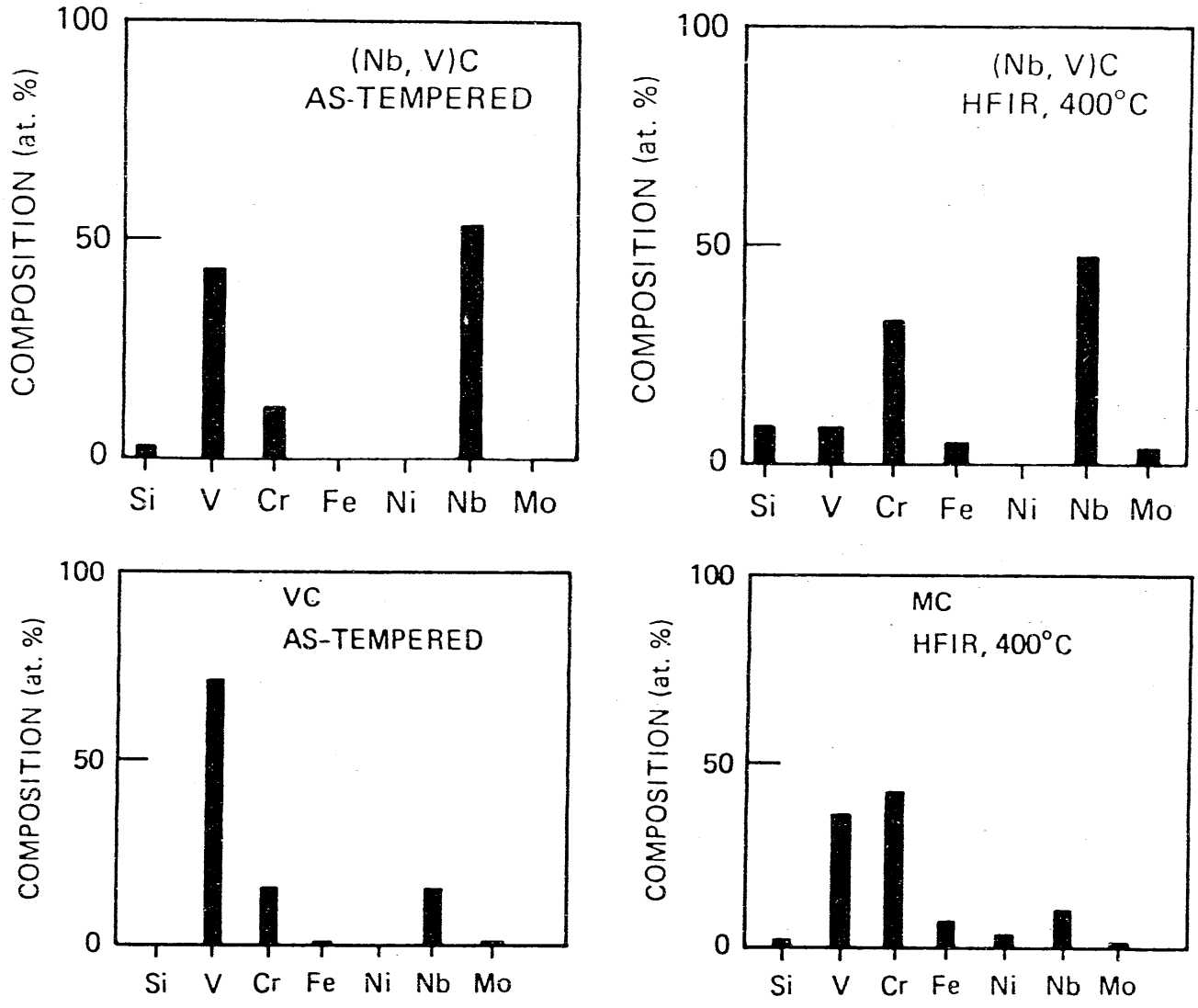

Fig. 12

Fig # 12
~~Fig. 12~~

ORNL-DWG 87M-7565R2

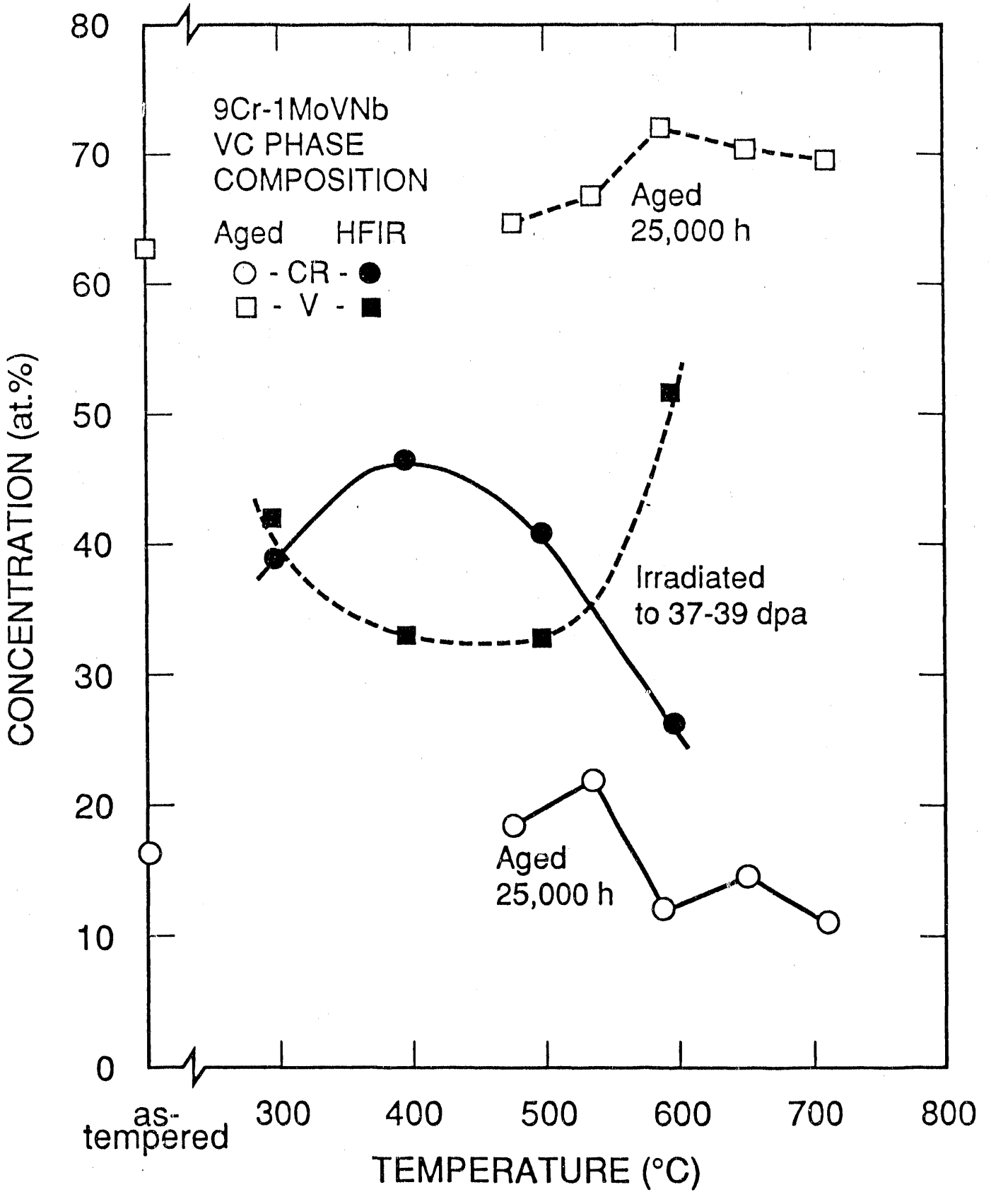

Fig. 13

ORNL-DWG 87M-7565R2

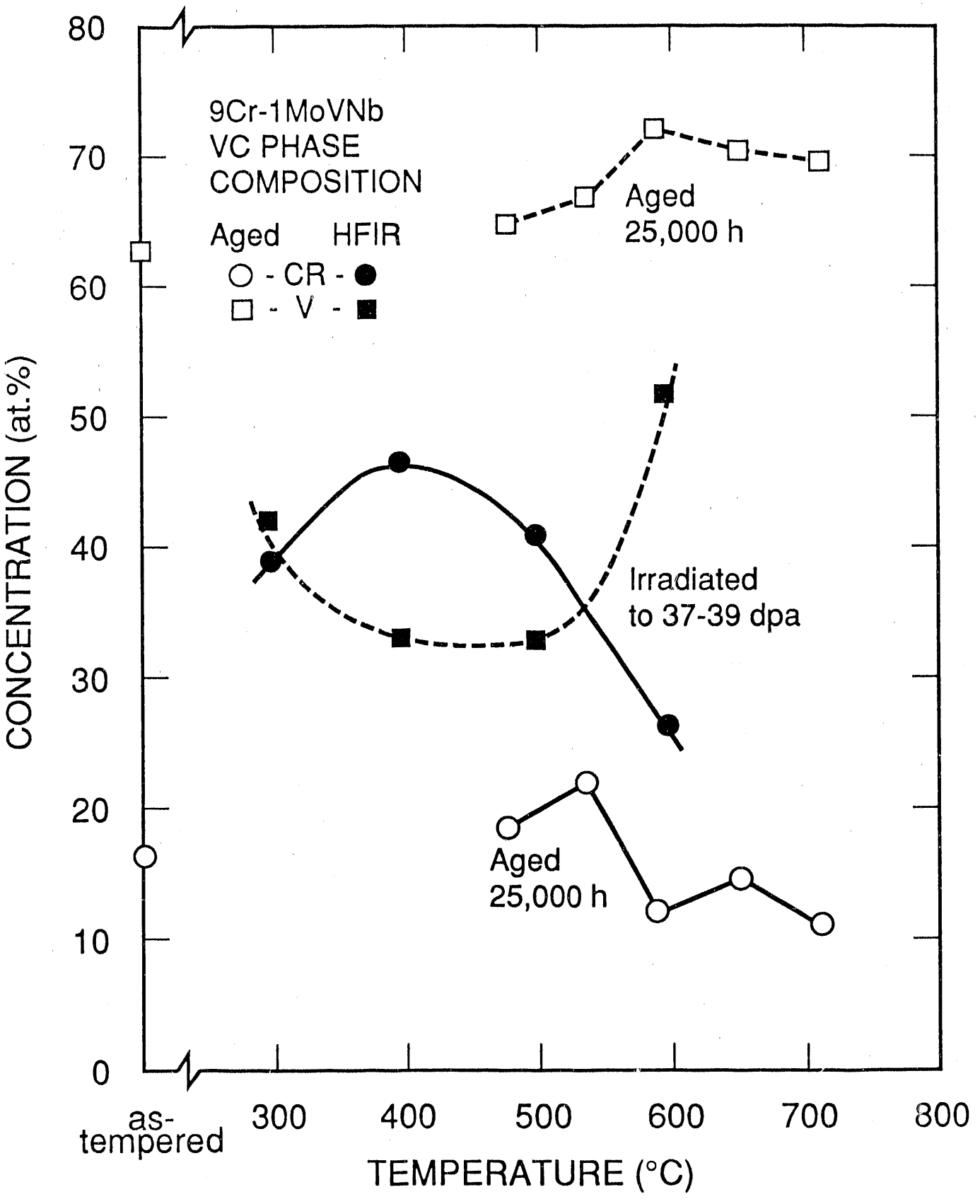

Fig. 13

END

DATE FILMED

12/18/90